Measurement of wavefront phase delay and optical density in apodized coronagraphic mask materials

Peter G. Halverson[*a], Michael Z Ftaclas[a], Kunjithapatham Balasubramanian[a],
Daniel J Hoppe[a], Daniel W. Wilson[a]

[a]Jet Propulsion Laboratory, California Institute of Technology,
4800 Oak Grove Drive, Pasadena CA 91109

ABSTRACT

The development of stellar coronagraphs for exoplanet detection requires apodized occulting masks to effectively remove the light from the central star while allowing planet light to propagate past. One possible implementation, a gray-scale mask, includes the placement of micron-scale neutral density light absorbing patterns using High Energy Beam Sensitive (HEBS) glass. A second implementation, binary masks, uses micron-scale diffractive/reflective patterns.

Coronagraph performance will be influenced by wavefront phase shifts introduced by the masks, hence accurate characterization of the fundamental optical properties, namely optical density (OD), phase advance/delay and optical constants of the material is needed for occulter design, development and modeling.

In this paper we describe an interferometric apparatus that measures wavefront phase advance/delay through grey-scale and binary masks as functions of wavelength and optical density, which is also measured. Results for HEBS gray-scale masks will be presented along with ellipsometric measurements of optical constants.
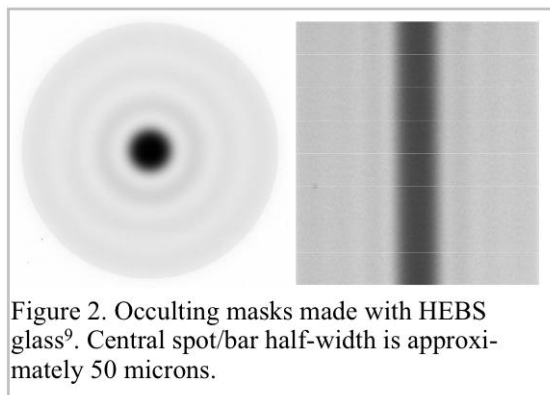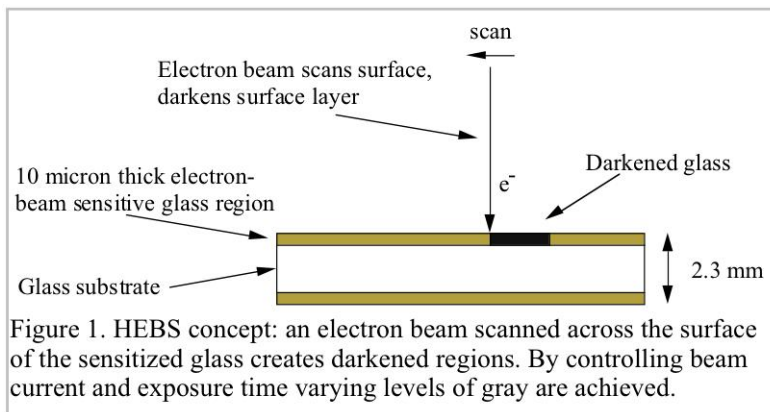
Keywords: Coronagraph occulting mask, neutral density pattern, gray scale photomask, High Energy Beam Sensitive (HEBS) glass, wavefront phase delay, extrasolar planet detection, exoplanet detection, ellipsometry, optical constants

1. INTRODUCTION

NASA's Terrestrial Planet Finder (TPF) missions[1] have been described elsewhere, and the program's coronagraph component (TPF-C) will be reviewed in another paper presented at this conference[2].

An important technological element of the coronagraph is the occulting mask, the "dark spot" that prevents starlight from reaching the coronagraph instruments (camera, spectrograph, etc.) while still allowing the light of a planet orbiting the star to pass through. The current TPF-C design calls for a gray-scale mask that features a carefully calculated darkness profile.

Figure 1. HEBS concept: an electron beam scanned across the surface of the sensitized glass creates darkened regions. By controlling beam current and exposure time varying levels of gray are achieved.

Ideally, the mask's amplitude transmission function would have a finite range of Fourier components that would diffract on-axis light (starlight) to a finite region in the conjugate plane, allowing the light to be completely blocked with a suitably shaped Lyot stop[3,4]. In practice, the transmission function of any real mask will have a wavelength-dependent amplitude portion as well as a non-uniform phase portion which depends both on wavelength and the amplitude transmission. This prevents a single mask and Lyot stop alone from achieving the high levels of starlight suppression required for TPF-C at even a single wavelength. The implementation of wavefront sensing and control alleviates[5] the phase transmission problem monochromatically to levels suitable for TPF-C, but this correction will itself have a problematic wavelength dependence[6,7].

Figure 2. Occulting masks made with HEBS glass[9]. Central spot/bar half-width is approximately 50 microns.

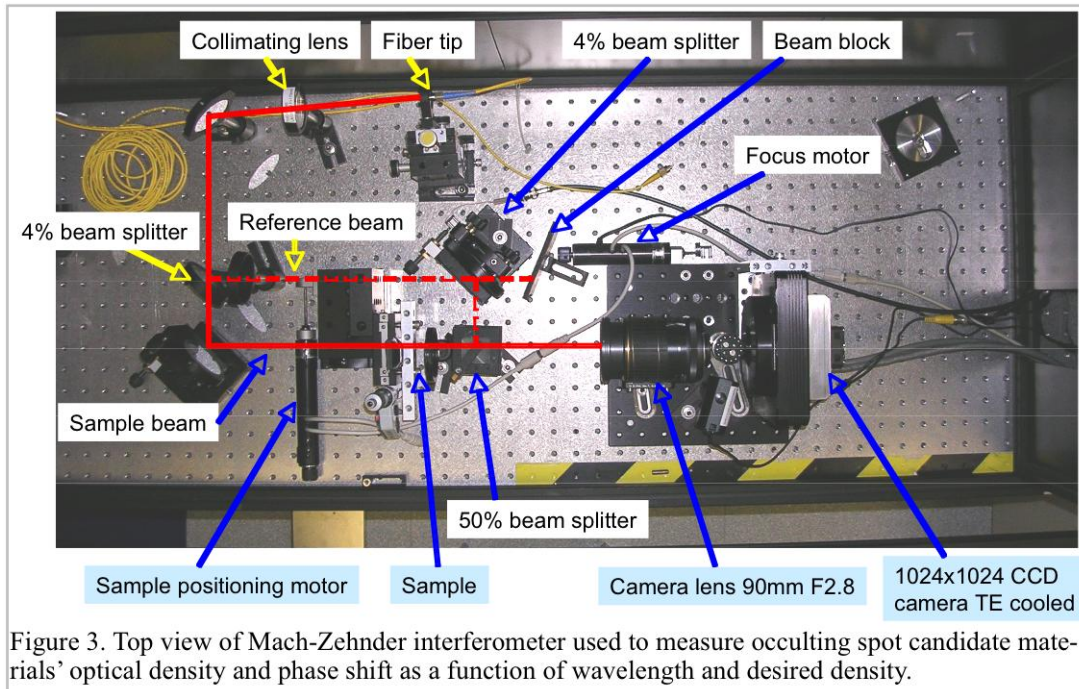[*]peter.g.halverson@jpl.nasa.gov; phone 626-287-3225; jpl.nasa.gov

Figure 3. Top view of Mach-Zehnder interferometer used to measure occulting spot candidate materials' optical density and phase shift as a function of wavelength and desired density.

Modeling coronagraph performance and designing a mask which diffracts as much on-axis light as possible onto the Lyot stop over the bandwidth of interest for TPF-C requires a knowledge of the phase and amplitude transmission of each of the candidate mask technologies. This knowledge would also allow incorporation of wavefront correction techniques to minimize the amount of light leakage. In most optical analyses of TPF-C, it is assumed that the optical density profile of the occulting mask is perfectly specifiable and wavelength independent. However "real" mask materials will inevitably have some wavelength dependance of O.D. The data presented here are currently being incorporated in higher fidelity iterations of TPF-C optical models.
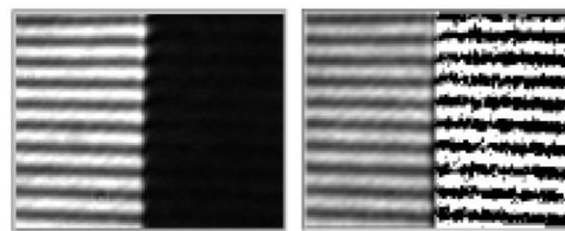

Figure 4. Example of phase shift of 785 nm light traversing a gray-scale mask that has two optical densities zones, O.D. 0 and O.D. 2.3. In the raw CCD image (left), fringes in the O.D. 2.3 zone are difficult to see due to zone darkness. The right image has had the dark zone enhanced to make the fringes visible. The fringes have a large offset (~1 radian) at the transition that can be seen as an upward step at the transition. (This image's HEBS glass, type GI85, is different from that used in figures 5 and 6.)

2. MASK MATERIAL

Currently, TPF-C has two "top" candidate technologies for fabrication of the occulting spot: High Energy Beam Sensitive (HEBS) glass[8] and metal-on-glass lithographic patterns. This paper addresses only the HEBS approach; metal-on-glass "binary" mask test results will be discussed in future communications.
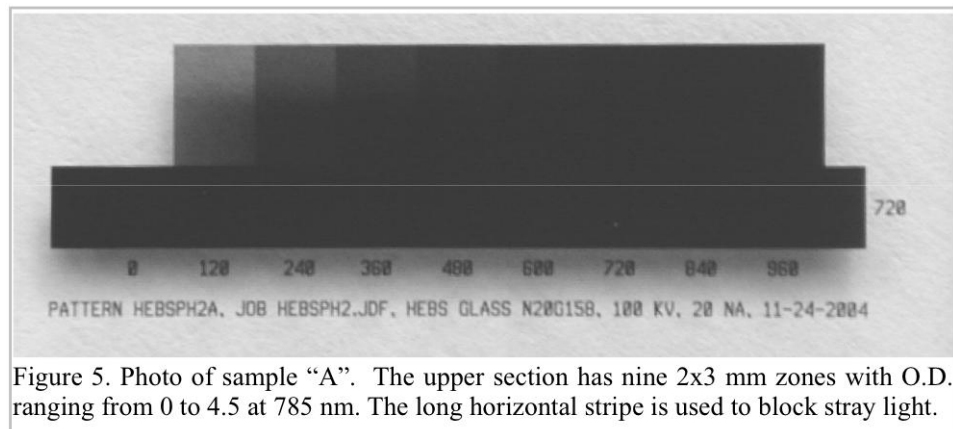

Figure 5. Photo of sample "A". The upper section has nine 2x3 mm zones with O.D. ranging from 0 to 4.5 at 785 nm. The long horizontal stripe is used to block stray light.

Previous experiments[9] conducted at JPL showed that HEBS glass, exposed with JPL's JEOL 9300FS electron beam system, satisfies key TPF-C needs:

- Continuously selectable optical densities (gray levels) with electron beam exposure.
- Sub-micron control of profile features (spot width, slope).
- Maximum optical densities exceeding 10^8.

Figure 1 sketches the HEBS concept while figure 2 shows actual occulting masks made by this process.

3. MEASUREMENT TECHNIQUE - PHASE AND O.D.

3.1. Apparatus

Candidate materials for the TPF-C occulting masks are characterized using the apparatus in figure 3. A Mach-Zehnder interferometer, collimated laser light is split into two arms, "sample" and "reference". After passing through the sample, light in the "sample beam" is recombined with the light of the "reference beam". It is then focused onto an Apogee AP47p CCD camera, where interference fringes in the combined light are recorded and written to disk in FITS format. Figure 4 illustrates the fringes and the apparent phase step due to a change in optical density.
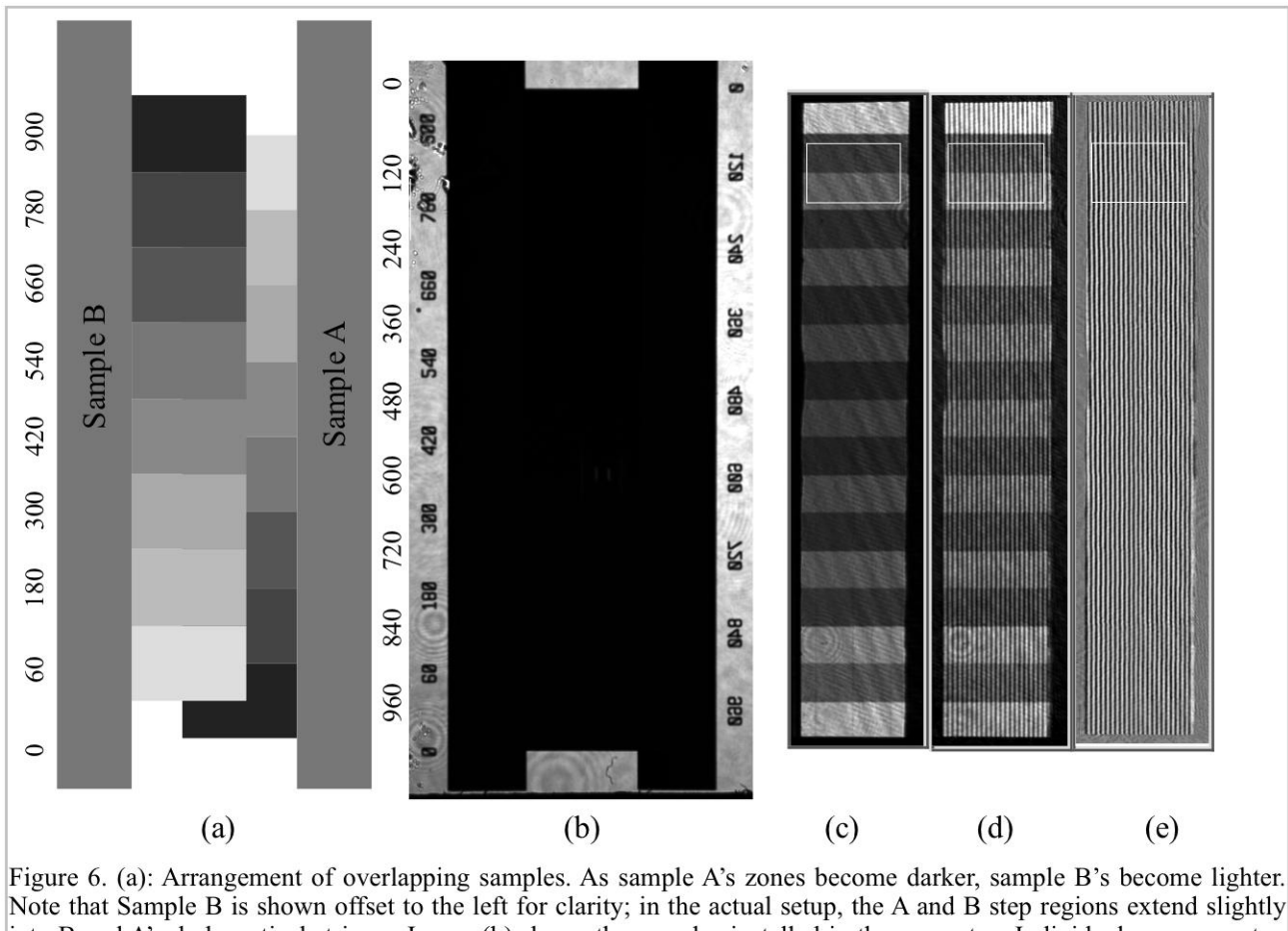

Figure 6. (a): Arrangement of overlapping samples. As sample A's zones become darker, sample B's become lighter. Note that Sample B is shown offset to the left for clarity; in the actual setup, the A and B step regions extend slightly into B and A's dark vertical stripes. Image (b) shows the samples installed in the apparatus. Individuals zones are too dark to be seen due to light flooding in from around the sample borders. In (c), the undarkened outer regions have been blocked, allowing the much dimmer electron beam darkened zones to be seen. Images (b) and (c) use only sample beam (also called the probe beam) light for illumination. In (d), reference beam light has been added, creating interference fringes. Additional processing, described in the text, enhances the fringes (e). The processing also removes certain defects visible in (c) such as ghost fringes (the faint diagonal fringes) and diffraction from dust and scratches (the circular patterns). The box in (c, d, e) specifies an analysis region for a single O.D. transition.

3.2. Samples

For ease of measurement, dedicated samples (figure 5) were produced, with 2x3 mm rectangular zones, each zone having a specific target O.D. The sharp transitions between zones provide the opportunity to more accurately measure O.D. and phase changes. However, the large range of optical densities, from OD 0 to 4.5 approaches the dynamic range of the CCD. Also, light scattering from dust and other defects and diffraction from stops further reduce the effective dynamic range.

To reduce the required dynamic range, it was decided to overlap two samples and orient them such that as one increases in optical density, the other decreases (figure 6a). The zone transitions are intercalated so that sample A's steps can be studied without confusion from sample B's steps. Between the transitions, the sample O.D. will be constant, so we expect the observed properties to change only at the transitions. The darkened layers of the two samples face each other and the small gap between the surfaces is filled with n=1.46 index matching fluid [10].

The image in figure 6d exhibits the interference fringes formed when reference beam light is added to the sample beam. Phase shifts are observed as small offsets at each transition between O.D. zones. An extreme example is figure 4, where the transition is from O.D. zero to O.D. 2.3. In this case a shift of about 1 radian is observed, large enough to be observed "by eye."
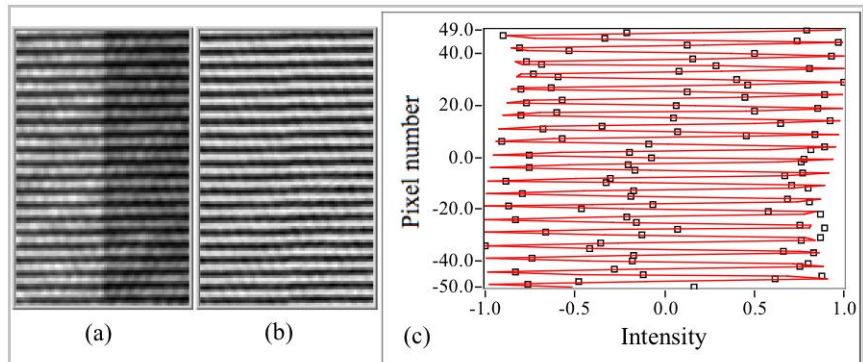

Figure 7. (a) Area selected in figure 6d, rotated left 90 degrees. Normalization yields image (b). (c): Sinusoidal fit to the first column of pixels in (b). The fits obtained for each column of pixels are plotted in the next figure.

4.Analysis

Analysis of the CCD image files is done with software written at JPL in LabVIEW. For each sample characterization run, the following images are recorded:

1. Sample-only image (no reference beam light).
2. Reference-only (no probe beam light).
3. Fringes image (sample and reference beam light used).
4. Probe beam only (sample beam with sample removed, no reference beam).
5. Dark (laser off).

These images are taken at each of the available laser wavelengths: 532, 635, 785 and 830 nm which span the range of interest for TPF-C.

Once the images have been acquired, they are enhanced for phase and O.D. analysis. The enhancement steps are:

1. Trim to include only the areas to be analyzed.
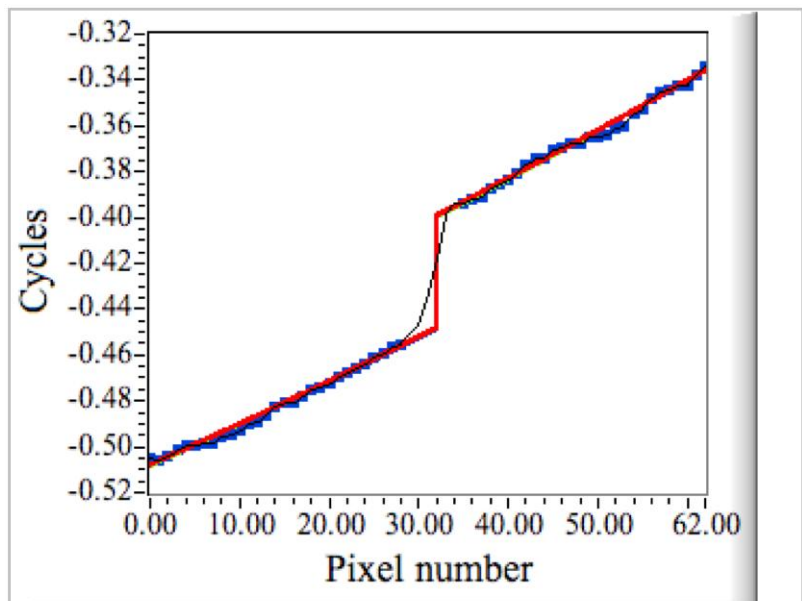2. Detect and limit "outlier" pixels, de-

Figure 8. Fit of 2nd order polynomial with adjustable step (thick red line) to the series of sinusoidal fits from figure 7c, showing a jump in phase at the O.D. transition. The thin black line represents all the sinusoidal fits; the blue squares indicate the sinusoidal fits that were used to find the polynomial-with-step fit.
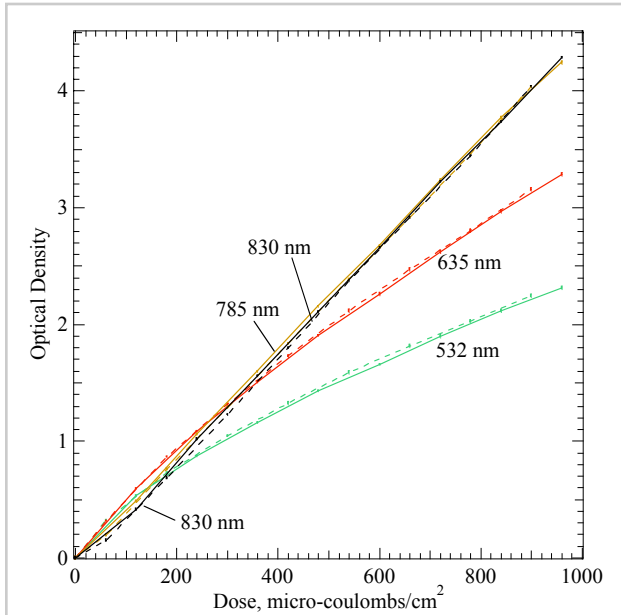
Figure 9. Measured O.D. for HEBS glass N20G158, darkened using 100 keV electron beam, 20 nA, at selected wavelengths. Solid/dashed lines indicate data from the A/B samples of figure 6.
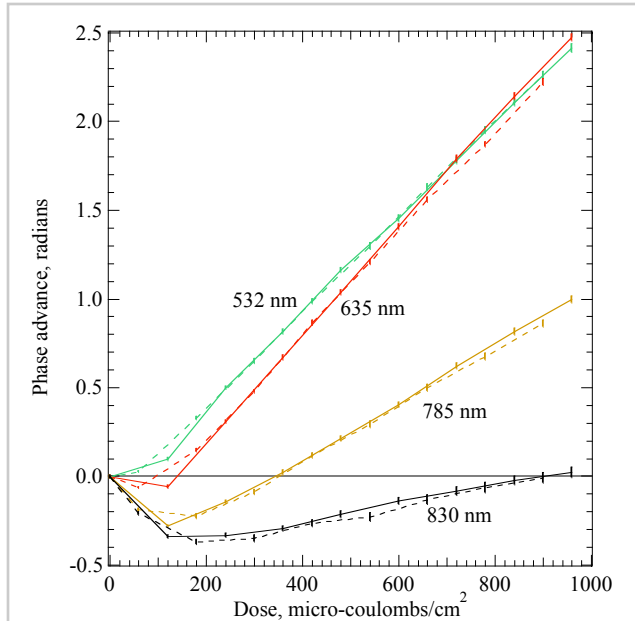

Figure 10. Phase advance, same samples as previous figure.

Figure 11. Phase advance as a function of O.D. This figure combines the data of the two previous figures.

fined to be brighter or darker than 99% of the image.

3. The dark image is subtracted from the sample-only, reference-only, fringes and probe-only images.
4. The sample-only image is normalized (divided by and rescaled) by the probe-only image yielding the <u>O.D. analysis image</u>, figure 6c.
5. The fringe-only image, figure 6d, is normalized (divided and rescaled) by the sum of the sample-only and reference-only images yielding the <u>fringes analysis image</u>, figure 6e.

The normalization steps, 4 and 5, are effective for the removal of image defects that are unrelated to the sample performance, such as the effects of dust, and ghost fringes due to parallel surfaces such as the CCD cover. The analysis images are then piecewise processed. Each piece is a sub-image that includes just one O.D. transition, and the zones of constant O.D. around it.

For the calculation of O.D., using the O.D. analysis sub-images we:

1. Deselect the transition zone itself, removing pixels that are affected by diffraction near the transition edge
2. Calculate the ratio of the average brightnesses of the two sub-regions. The change in O.D. is $\log_{10}$ of the brightness ratio.
3. Since each sub-image analysis yields a <u>change</u> in O.D., we cumulatively sum the changes to obtain the actual O.D. of a given zone.
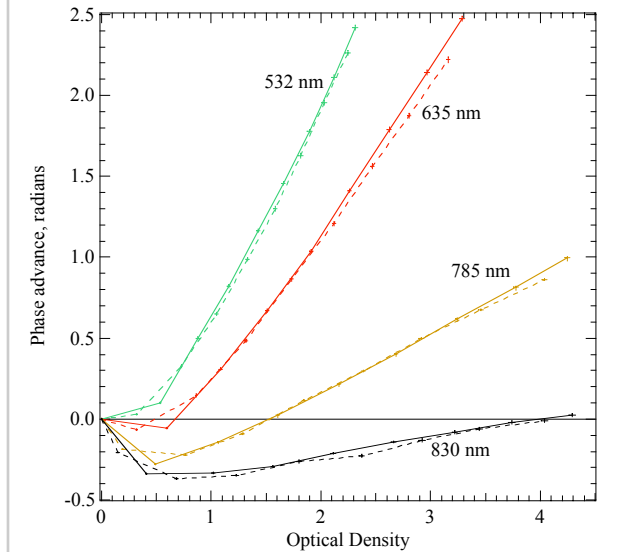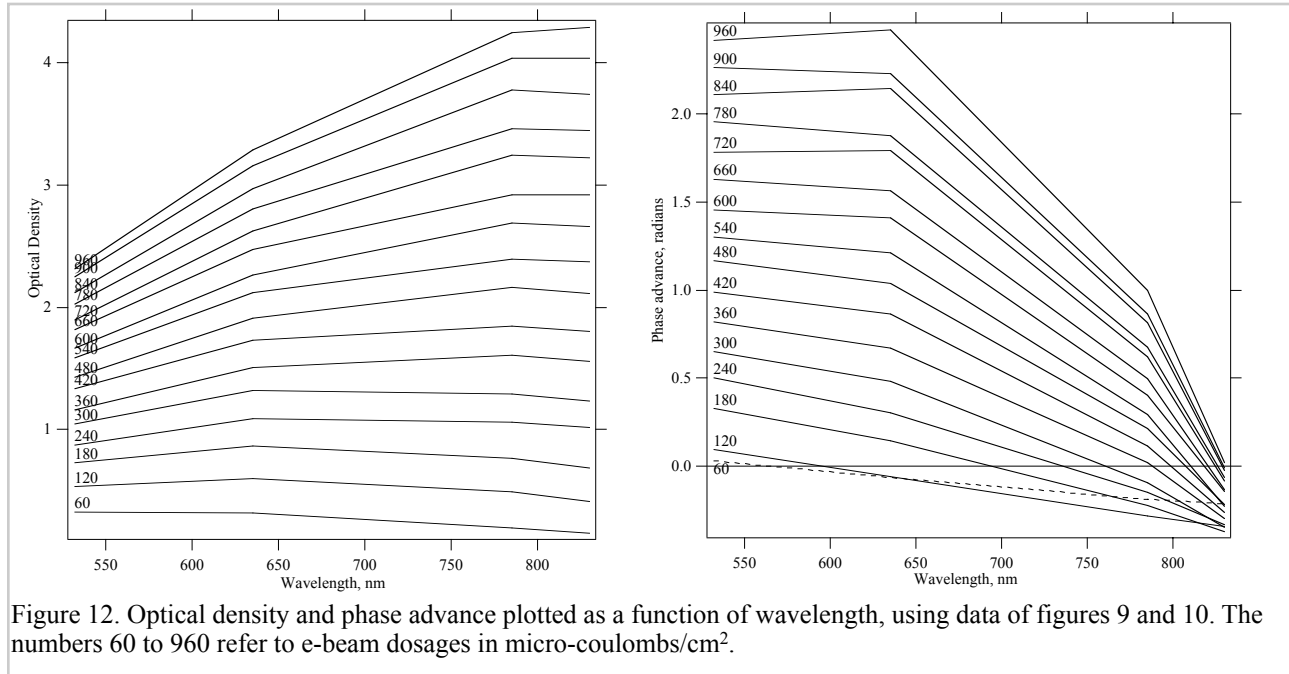
Figure 12. Optical density and phase advance plotted as a function of wavelength, using data of figures 9 and 10. The numbers 60 to 960 refer to e-beam dosages in micro-coulombs/cm^2.

The O.D. values reported here are all relative to the O.D. of the non-irradiated HEBS glass, which has a non-zero intrinsic absorption which would not affect the functionality of an occulting spot or Lyot stop made from this material.

The phase shift calculation begins with a sub-image as in figure 7b where we:
1. Select the leftmost column of pixels and fit a sinusoid to the vector of pixel brightnesses, figure 7c.
2. This fit is performed for each pixel column.
3. The phase of each fit from the previous step is plotted in figure 8. Using these phases (excluding those close to the transition's diffraction pattern), a polynomial with an adjustable step in the center is fit. The resulting fit's step size is taken to be the phase shift for that O.D. transition. Using a polynomial, as opposed to linear, fit is necessary to account for low spatial frequency variations in the HEBS glass thickness.
4. Since each sub-image analysis yields a <u>change</u> in phase, we cumulatively sum the changes to obtain the actual phase of a given zone.

The phases reported in this paper are relative to the phase delay of the non-irradiated HEBS glass. Phase <u>advance</u> indicates an decrease in the number of wavelengths needed by the probe light to traverse the sample.

5. RESULTS - PHASE AND O.D.

The results of measurements made with the samples shown in figure 6 are shown in figures 9 through 12. As expected, the darkness of the glass increases monotonically with electron beam exposure (figure 9). However the phase delay initially increases with exposure but then reverses and becomes a phase advance at higher exposures (figure 10). This can be interpreted as the dark layer's refractive index being greater than that of unexposed HEBS for small exposures, then becoming less than unexposed HEBS as the exposure is further increased. Figure 11 combines the O.D. and phase data.

Looking at the same O.D. and phase data as a function of wavelength, figure 12, we see that as the wavelength increases, the O.D. is increasing while the phase advance is decreasing. This is consistent with the predictions of the Kramers-Kronig relations. More detailed absorption data is currently being acquired, which may further clarify this material's behavior.

The results presented in this section should be considered specific to the particular formulation (type N20G158) of HEBS glass tested, to the electron beam energy (100 keV), and beam current (20 nA). Canyon Materials made this version of HEBS glass to provide a degree of control over the spectral behavior the mask. This formulation, exposed to

low-energy (12~15 keV) electrons is expected to have maximum absorption at 480 nm, while exposure to high energy (~100 keV) electrons will shift the peak to 900 nm, consistent with figure 12. Beam current may also be significant, due to heating.

6. FURTHER STUDIES: ELLIPSOMETRY, SURFACE PROFILE

Because early O.D. versus phase measurements indicated that HEBS glass is more complicated than previously thought, a parallel series of tests was initiated which will be discussed below.

6.1. Sample material

The tests described in this section were done on HEBS glass type GI85, with a 10 micron thick HEBS layer, exposed to a 100 keV electron beam, as described in reference[9]. (Usually GI85's sensitive layer is three microns thick; this glass was special.) This is not the glass used in the previous sections of this paper, but we suspect that the qualitative features of the results below apply to the HEBS family of products. To accommodate the sample area requirements of the ellipsometer, a sample was prepared with eight 5 mm square zones of progressively higher electron beam exposure as shown in figure 13.
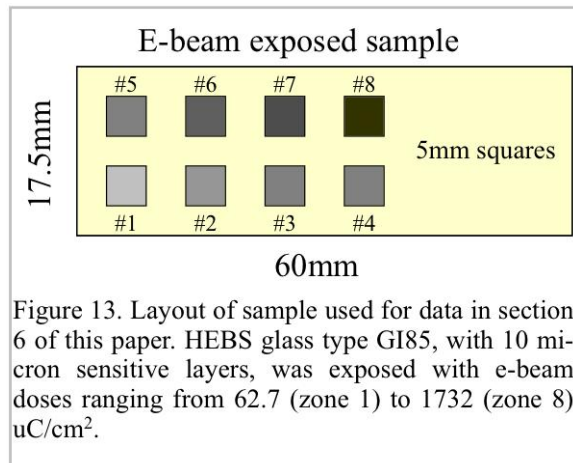

Figure 13. Layout of sample used for data in section 6 of this paper. HEBS glass type GI85, with 10 micron sensitive layers, was exposed with e-beam doses ranging from 62.7 (zone 1) to 1732 (zone 8) uC/cm^2.

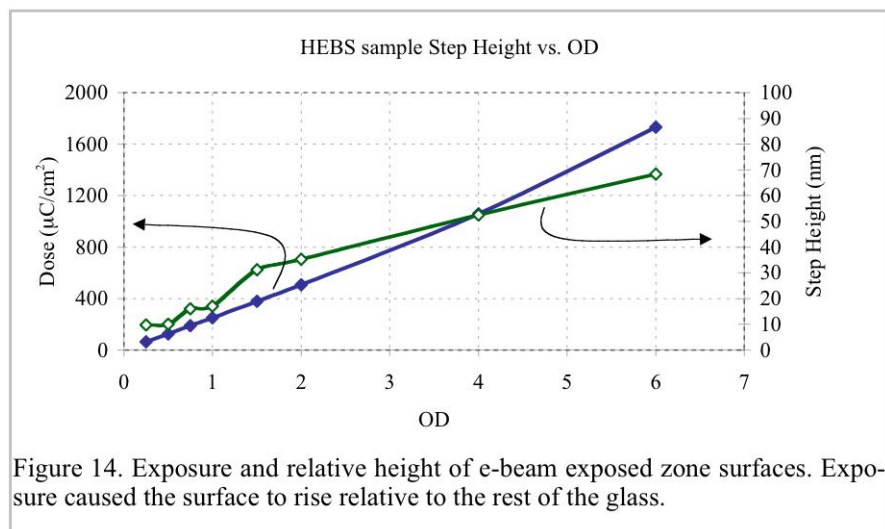Figure 14. Exposure and relative height of e-beam exposed zone surfaces. Exposure caused the surface to rise relative to the rest of the glass.

6.2. Surface Profile scan

An early question arising from the phase data was whether the electron beam might be removing material from the mask. To answer this, the sample of figure 13 was scanned with a Tencor AlphaStep 500 profilometer. The results, figure 14, show that the e-beam exposure actually *increases* the surface height (the opposite of creating a hole), presumably by introducing dislocations. This effect by itself does not explain the retard/advance behavior of exposed HEBS.

6.3. Ellipsometry

The sample was sent to J.A. Woolam Co. where the optical constants n and k of the sample of figure 13 were measured with a VASE spectroscopic ellipsometer[11]. Due to the roughly 10 micron thickness of the layer and an observed 150 nm graded index surface layer on the HEBS layer, the absolute measurement of n and k is subject to errors due to imperfect model fits. However, the trends are within reason and consistent with the OD and phase measurements made with interferometry, described in sections 2 to 5.
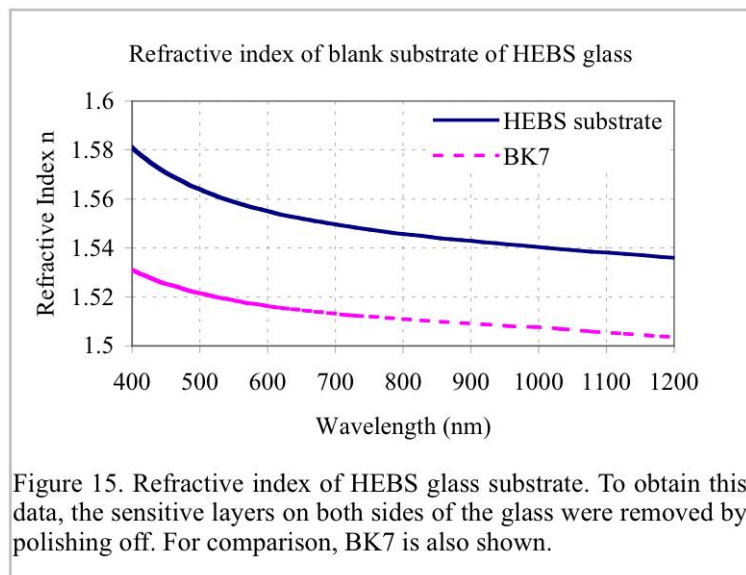

Figure 15. Refractive index of HEBS glass substrate. To obtain this data, the sensitive layers on both sides of the glass were removed by polishing off. For comparison, BK7 is also shown.

In Figure 15, the HEBS substrate refractive index is shown, together with that of BK7 as measured by ellipsometry. Refractive index and extinction coefficient as a function of electron beam exposure, for a wavelength of 785nm, is plotted in figure 16. It is interesting to note that the change in refractive index with e-beam exposure exhibits three distinct regimes of material interaction with electron beam dose. Initially, n increases slightly and then drops rapidly with exposure. Above 500 uC/cm^2 exposure, the drop in refractive index slows down as does the increase in extinction coefficient.

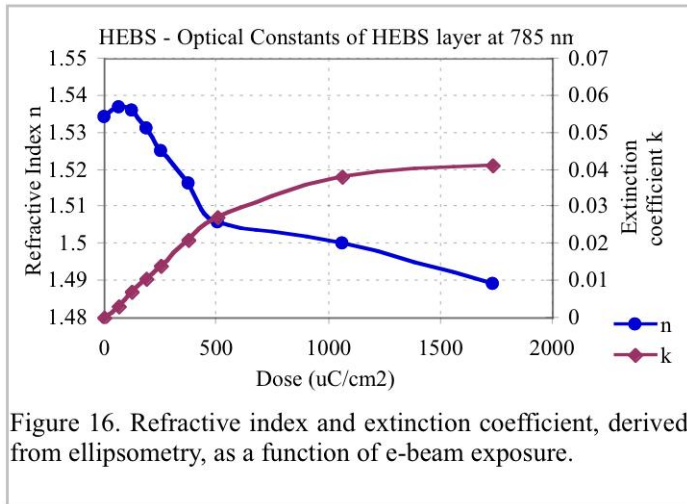Using these optical constants, one can model the phase of transmitted light through the different exposure regions. Phase advance/delay with respect to unexposed HEBS glass is plotted in figure 17.

Figure 16. Refractive index and extinction coefficient, derived from ellipsometry, as a function of e-beam exposure.

The phase shows the same trend as that measured by interferometry reported in figure 10, though the absolute values differ. Differences can be explained qualitatively as due to:
• A somewhat different HEBS formulation.
• Errors in the thickness estimate of the HEBS layer.
• Imperfect model fits of the layer structure.

Figure 18 shows the refractive indices and extinction coefficients of the HEBS material as a function wavelength for various levels of electron beam exposure, while figure 19 shows the measured optical densities.

An interesting aspect of the HEBS glass is that it is composed of nominally 10 micron thick sensitive layers on both sides of the
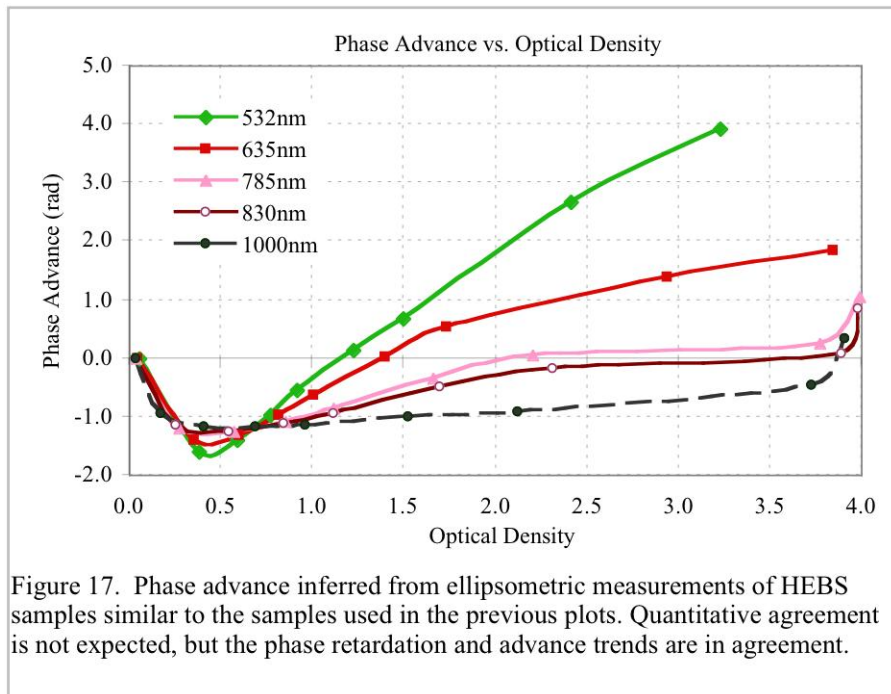

Figure 17. Phase advance inferred from ellipsometric measurements of HEBS samples similar to the samples used in the previous plots. Quantitative agreement is not expected, but the phase retardation and advance trends are in agreement.

substrate. As a consequence of the large thickness and interference effects, the transmitted light exhibits a modulation as a function of wavelength as shown in figure 20. Such a modulation is likely to affect the performance of the mask in broad band illumination. One potential way to eliminate the problem is to remove the unneeded bottom 10 micron layer by polishing it off and then applying an anti-reflective coating. This would eliminate an unwanted ghost reflection and increase mask throughput.

7. CONCLUSION

While HEBS glass material is still a promising candidate for the TPF-C's occulting mask, its wavelength dependance complicates analysis and, in the absence of any improvements, would reduce the instrument's usable bandwidth. Efforts to broaden the absorption band are underway. If successful, these are likely to result in better phase shift behavior.

An alternative technology, binary masks, are currently being tested. However these will also have a strong wavelength (and polarization) dependance for transmittance and phase advance/delay.
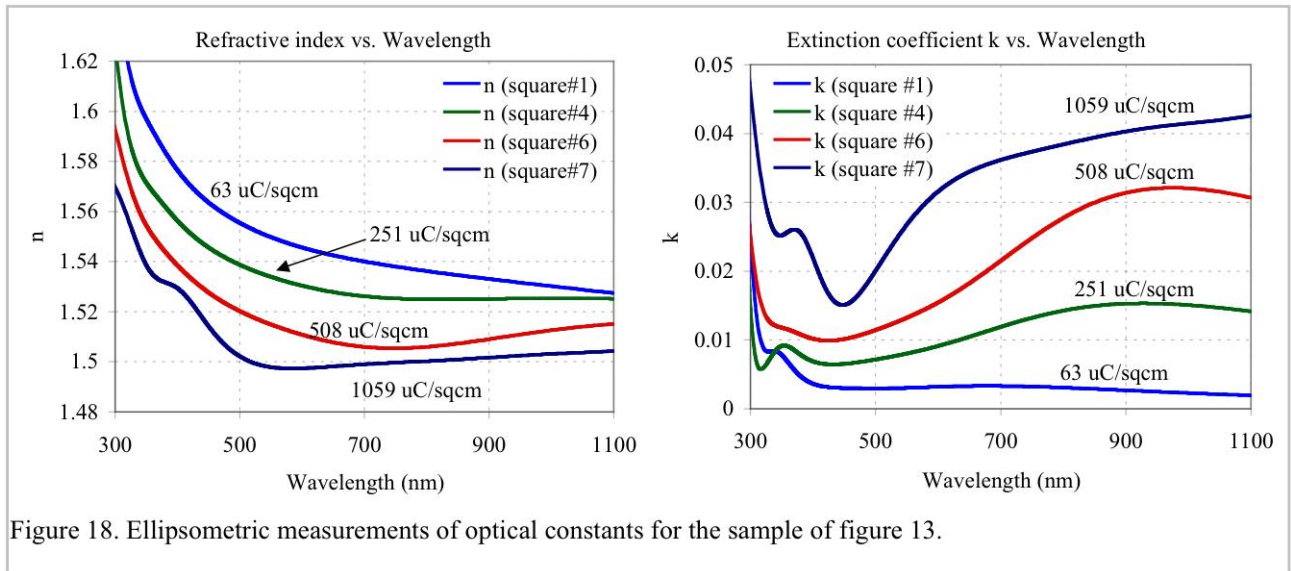

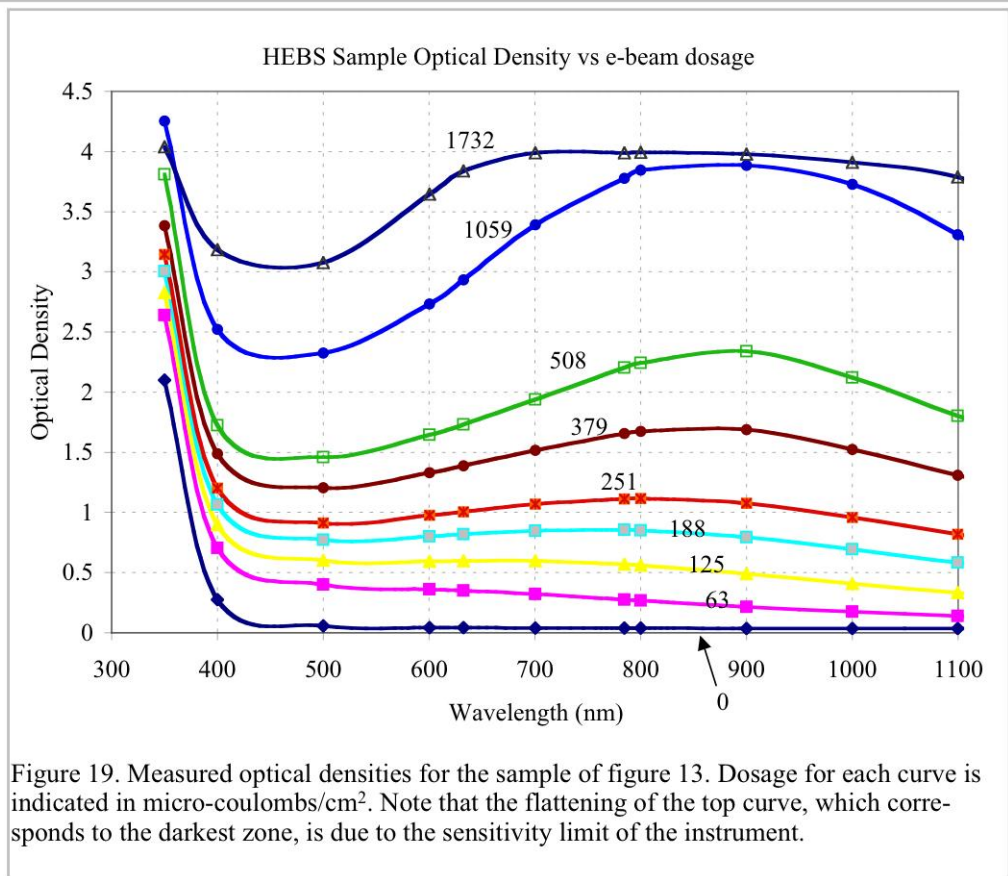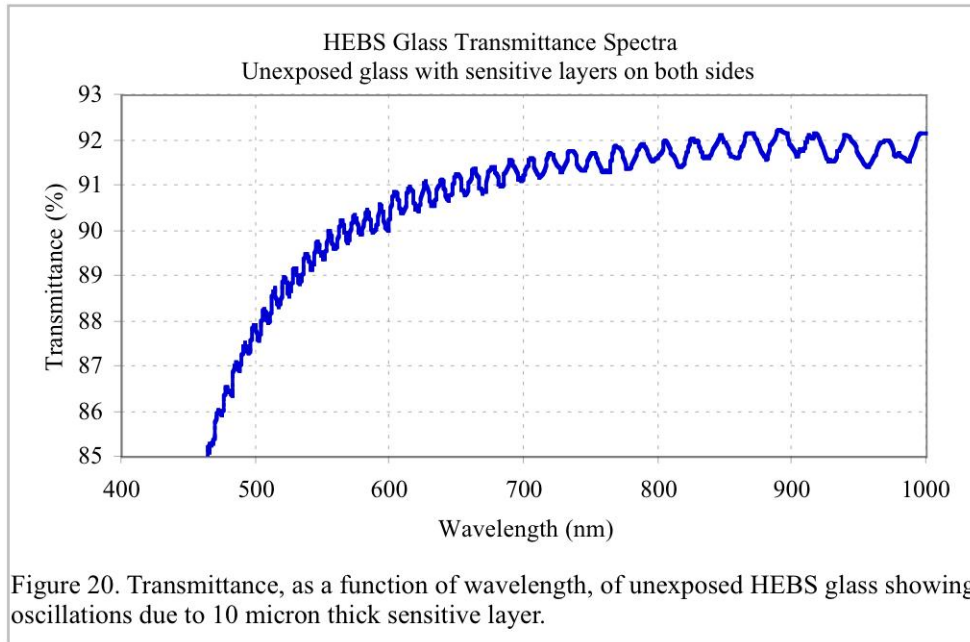Figure 18. Ellipsometric measurements of optical constants for the sample of figure 13.

Figure 19. Measured optical densities for the sample of figure 13. Dosage for each curve is indicated in micro-coulombs/cm^2. Note that the flattening of the top curve, which corresponds to the darkest zone, is due to the sensitivity limit of the instrument.

Figure 20. Transmittance, as a function of wavelength, of unexposed HEBS glass showing oscillations due to 10 micron thick sensitive layer.

ACKNOWLEDGMENT

REFERENCES

[1] http://planetquest.jpl.nasa.gov/TPF/tpf_index.html

[2] V.G. Ford. "Terrestrial Planet Finder Coronagraph 2005: overview of system design studies and technology development", SPIE **5905**, 2005. (This conference.)

[3] M.J. Kuchner, W.A. Traub. "A coronagraph with a band-limited mask for finding terrestrial planets," ApJ **570**, 900-908, 2002.

[4] M.J. Kuchner, D.N. Spergel. "Notch filter masks: practical image masks for planet finding terrestrial planets", ApJ **594**, 617-626, 2003

[5] J.T. Trauger, *et al.* "Laboratory demonstration of high-contrast imaging technologies and algorithms for space coronagraphy", SPIE **5905**, 2005. (This conference.)

[6] O.P. Lay, J.J. Green, D.J. Hoppe, S.B. Shaklan, "Coronagraph mask tolerances for exo-earth detection," SPIE **5905**, 2003. (This conference.)

[7] S.B. Shaklan, L.F. Marchen, J.J. Green, "The terrestrial planet finder coronagraph error budget," SPIE **5905**, 2003. (This conference.)

[8] Canyon Materials, Inc., San Diego, California, USA. http://www.canyonmaterials.com/hebs.html

[9] D.W. Wilson, P. D. Maker, J.T. Trauger, T.B. Hull. "Eclipe apodization: realization of occulting spots and Lyot masks," Proc. SPIE **4860**, 361-370, 2003.

[10] Cargille #19569, http://www.cargille.com/specimmerliq.shtml

[11] J.A. Woollam Co. Inc, Lincoln, Nebraska http://www.jawoollam.com/